Effect of drawing stress on mesophase structure formation of poly(ethylene 2,6-naphthalene dicarboxylate) fiber just after the neck-drawing point

Kyoung-Hou Kim,[†] Ryo Aida,[‡] Young-Ah Kang,[§] Toshifumi Ikaga,[‡] Yutaka Ohkoshi,[*,‡] Isao Wataoka,[#] Hiroshi Urakawa[#]

[†]*Textile & Consumer Goods Examination Division, Korean Intellectual Property Office, Government Complex Daejeon Building 4, 189, Cheongsa-ro, Seo-gu, Daejeon 302-701, Republic of Korea;* [‡]*Faculty of Textile Science and Technology, Shinshu University, 3-15-1 Tokida, Ueda, Nagano 386-8567, Japan;* [§]*Research Institute of Human Ecology, Dong-A University, 840 Hadan-dong, Saha-gu, Busan 604-714, Republic of Korea;* [#]*Graduate School of Science and Technology, Kyoto Institute of Technology, Goshokaidoucho, Matsugasaki, Sakyo-ku, Kyoto 606-8585, Japan*

ABSTRACT

The structural development of poly(ethylene 2,6-naphthalene dicarboxylate) (PEN) fibers was analyzed by *in situ* X-ray diffraction and fiber temperature measurements. The PEN fiber was drawn continuously under three drawing stresses, where the neck-drawing point was fixed accurately by CO_2 laser irradiation heating. The developed crystal structures of the drawn fibers depended on the drawing stresses, that is, only the α-crystal was obtained under a drawing stress of 148 MPa, an α-rich mixed crystal was obtained for 54 MPa, and a β-rich mixed crystal was obtained under 23 MPa stress. Fiber containing over 70% β-crystal was obtained in the third case. Orientation-induced crystallization rates (K) and crystallization induction times (t_0) were estimated for the three drawing stresses: K= 2210 s^{-1} and t_0= 0.5 ms for 148 MPa, K= 940 s^{-1} and t_0= 1.0 ms for 54 MPa, and K= 655 s^{-1} and t_0= 4.0 ms for 23 MPa. In addition, the drawing stress acted as a definitive influence not only on the resulting crystal form but also on the chain conformation of the mesophase structure. The *d*-spacing of the (001') diffraction increased with drawing stress, and the longer (001') spacing generated the α-crystal while the comparatively shorter (001') spacing yielded the β-crystal. The *d*-spacings of 1.27 and 1.23 nm for the drawing stresses of 148 and 23 MPa, respectively, were somewhat shorter than the *c*-axis lengths of the α- and β-crystals of 1.32 and 1.27 nm, respectively.

Keywords:

Poly(ethylene 2,6-naphthalene dicarboxylate), mesophase structure, CO_2 laser-heated drawing

1. Introduction

Poly(ethylene 2,6-naphthalene dicarboxylate) (PEN), which contains a naphthalene ring in its backbone, has a higher glass-transition temperature (T_g) and melting temperature (T_m) compared to poly(ethylene terephthalate) (PET). Due to the stiff molecular chains of PEN, it is used in making high performance sailcloth. PEN is also used for manufacturing high performance fibers such as tire cords that have very high modulus and better dimensional stability than polyester and nylon fibers.

PEN is reported to have two different crystal structures, the α- and β-forms. The α-crystal is triclinic, with unit cell parameters of a=0.651 nm, b=0.575 nm, c=1.32 nm, α= 81.33°, β= 144°, and γ= 100°.[1] The β-crystal is also triclinic but has significantly different unit cell parameters of a=0.926 nm, b=1.559 nm, c=1.273 nm, α= 121.6°, β= 95.57°, and γ= 122.52°.[2] The α- and β-crystal densities are 1.407 and 1.439 g/cm^3, respectively. The β-crystal has a higher crystal density and shorter *c*-axis length than the α-crystal. In other words, the molecular chains in the β-crystal are densely packed but are not fully extended along the chain axis. Buchner et al. have suggested that every naphthalene ring is twisted around the chain axis by about 180° in the β-crystal.[2] It was also reported that the β-crystal can be formed when the isotropic melt is crystallized at temperatures higher than 220°C.[2,3]

There have been previous studies on hot-drawing and cold-drawing processes for PEN fibers and films,[4,5] wherein the drawability of amorphous PEN was reported to depend on the molecular weight and strain rate. The structural changes upon neck drawing of amorphous PEN films have been investigated through off-line measurements using synchrotron X-ray radiation,[4,6] which revealed the appearance of smectic order with a period of 1.25 nm corresponding to a chain repeat length associated with a sinusoidal conformation of the polymer chains. It was 5% shorter than the chain repeat length of a more extended α-

conformation. In a previous study,[7] we conducted *in situ* characterization during CO_2 laser-heated drawing and found a temporal appearance of meridional (001') diffraction within a few microseconds after the onset of necking, indicating that the mesophase structure was formed in the initial stage of the fiber structure development of PEN. To the best of our knowledge, this was the first finding of mesophase structure by *in situ* measurement in the continuous drawing of PEN fibers. The *d*-spacing of the (001') diffraction was 1.230±0.003 nm, which was shorter than the *c*-axis lengths of both α- and β-crystals.

The CO_2 laser-heated drawing conducted by our research group permits *in situ* characterization around the location where necking occurs. This location can be nearly fixed within 0.2 mm since the laser irradiation can heat the running fiber rapidly with no contact. The fiber structure development in the vicinity of the necking location has been investigated through *in situ* characterization using a laser drawing system connected to the synchrotron X-ray scattering apparatus of the SPring-8 facility for PET, poly(trimethylene terephthalate) (PTT), poly(ethylene naphthalate) (PEN), and poly(vinylidene fluoride) (PVDF) fibers.[7-13] For PET and PEN, it was revealed that a fibrillar-shaped structure having a smectic-like two-dimensional order was developed prior to orientation-induced crystallization. This was based on the fact that the meridional (001') diffraction was observed immediately after necking and then disappeared after a few milliseconds. The fibrillar structure supports the whole body of the fiber under an externally applied stress, and is very important in the development of its mechanical properties.

We previously described the fine structure and properties of PEN fibers obtained by laser-heated drawing in order to realize high strength and modulus.[14] It was observed that the necking behavior varied with the draw ratio and drawing stress during the laser-heated drawing. Subsequently, different crystal structures were obtained as a function of the drawing stress. In the present study, in order to investigate the fiber structure development in PEN

fibers with various draw ratios and drawing stresses, *in situ* WAXD measurements using synchrotron radiation were conducted during the CO_2 laser-heated drawing. The quasi-smectic-like fibrillar structure development before crystalline structure formation was characterized, and the subsequent crystal modification based on the pre-crystallization structure was investigated.

2. Experimental

2.1. Fundamentals of in situ measurements. The *in situ* measurement system used in the present study is shown schematically in Figure 1(a). Details of the *in situ* measurements can be found in previous papers.[7-13] As described in detail elsewhere, the running fiber was heated through three-directional irradiation by four mirrors using a CO_2 laser beam generated by a PIN-20S laser source manufactured by Onizca Glass Co. Ltd, as shown in Figure 1(b). This can minimize the cross-sectional distribution of temperature in the fiber. The laser source had a rated power of 20±1 W with a beam diameter of 5 mm. Highly stable neck drawing wherein the neck-drawing point hardly fluctuates within 1 mm is possible for the laser-heated drawing, because the laser irradiation can heat the running fiber rapidly and homogeneously with no contact. The applied laser power was measured using a PW-250 powermeter from SYNRAD Co. Ltd. and the drawing stress was measured with sensors of 100 and 20 gf using a HS-1500S tensionmeter (EIKO SOKKI Co. Ltd.) and a TTM-201 tensionmeter (Toray Co. Ltd.), respectively. The running fiber was drawn by a speed differential between the feed and take-up rollers. X-ray diffraction images and fiber temperature were obtained as a function of elapsed time *t*, which was calculated on the basis of distance *D* between the measurement and necking points, divided by the fiber running speed *v*. The distance *D* was controlled by shifting the necking position using a traveling

mirror unit, as described previously.[7-13]

2.2. Material and melt-spinning. The PEN pellets ([η]=0.94 dl/g) used in the present study were melted and extruded through a single-hole spinneret of 1.0 mm diameter (L/D=5) at 310°C. The throughput rate was controlled to 4.0 g/min. The spinning line was not equipped with an air quenching apparatus. The fiber was taken up at a speed of 384 m/min. The as-spun PEN fiber had a diameter of 103±2 μm, and revealed an amorphous halo in the WAXD pattern.

2.3. Fiber temperature measurement. The fiber temperature was measured by means of an infrared thermo-spot sensor (TNZ7N2-J0-5K1-2 type, Japan Sensor Co., Ltd), equipped with a HgCdTe sensor and an interference filter. The response time was 10 ms. The interference filter transmits a wavelength of 5.78±0.1 μm, which corresponds to the absorbance band of C=O stretching. *In situ* fiber temperature measurement was conducted in the same manner as in previous studies.[7-13]

2.4. Neck drawing and time resolution. We selected three stable drawing conditions, with drawing stresses of 148, 54, and 23 MPa, as presented in Table 1. The laser power for each condition was chosen to minimize the fluctuation of necking point.

The neck-drawing point was observed by a TK-C1461 CCD camera from VICTOR Co equipped a TV-1M telecentric lens from the OPTART Co. The time resolution was estimated for every measurement point. The time resolution was obtained by dividing the position resolution of the necking by the fiber running speed, and the position resolution ($W_{x\text{-}ray}$) was calculated using Eq. (1) using the width of the X-ray beam (W_{beam}), the fluctuation of the neck-deformation point (W_{neck}), and the length of the neck deformation (W_{deform}). W_{neck} and W_{deform} were estimated by image analysis of the CCD camera images around the neck-drawing point. Here, time resolutions of 1.5, 1.9 and 1.8 ms were respectively obtained for drawing stresses of 148, 54, and 23 MPa.

$$W_{X-ray} = \sqrt{{W_{beam}}^2 + {W_{neck}}^2 + {W_{deform}}^2} \quad (1)$$

2.5. Wide angle X-ray diffraction measurement. The 40B2 beam line of the synchrotron radiation X-ray source in SPring-8 was used in this study. The X-ray beam diameter (W_{beam}) was 0.2 mm and the applied wavelength was 0.08 nm. A wide angle X-ray diffraction (WAXD) image was taken with a 3000×3000 pixel imaging plate in a 400 mm long vacuum chamber with an exposure time of 480 s. The sample-to-detector distance was calibrated using the diffraction pattern of lead dioxide (PbO_2) and hexamethylenetetramine ($C_6H_{12}N_4$). The necking point was located by the transmitted X-ray intensity profile through an ion chamber. The diffraction intensity profile for a polyimide film mounted in the vacuum chamber was used as a reference profile by subtracting a blank image. Additional details on the *in situ* WAXD measurement can be found in our previous reports.[7-13] The position θ_0 and the half width σ were determined by fitting with a Gauss function (2). The beam divergence effect on σ was corrected with the width of the intensity profiles of PbO_2. The *d*-spacing *d* and structure size *D* were calculated by Bragg's equation (3) and Scherer's equation (4), respectively, with a constant *k* value of 0.918.

$$I(\phi) = I_0 \exp\left\{-4\ln 2 \cdot \left(\frac{\theta - \theta_0}{\sigma}\right)^2\right\} \quad (2)$$

$$2d \sin\theta_0 = \lambda \quad (3)$$

$$D = \frac{k\lambda}{\sigma \cos\theta_0} \quad (4)$$

3. Results and discussion

3.1. Shape of Necking. The morphological change of the running fiber around the necking point was monitored using the CCD camera. Captured images are shown in Figure 2 wherein the width of the images is 3.7 mm. The length of the neck-deformation region increased with decreasing drawing stress, and was about 0.3 mm for 148 MPa and about 0.9 mm for 23 MPa. As presented in Table 1 and reported in the previous study,[14] a fine-tuned higher laser irradiation power was required for a lower drawing stress (23 MPa) with a longer neck-deformation region, while the high drawing stress (148 MPa) condition was stably attained with a comparatively low laser irradiation power.

3.2. Fiber temperature. Figure 3 shows the fiber temperature profile with distance (a) and elapsed time (b) from the necking point, designated as the origin of the horizontal axis, and the shaded region of (a) denotes the irradiation region of the laser beam. The fiber temperature was measured twice for each condition to confirm experimental reproducibility, and both results are shown in the figure. The fiber temperatures start to increase at the entrance of the laser irradiation region, and increase steeply up to about 110°C at the onset of neck deformation, which is located around the laser beam axis. The starting temperature for the necking lies close to the glass transition temperature (T_g) of PEN of 120°C.[5] The fiber temperature increased rapidly at the necking point by exothermic heat accompanied with plastic deformation up to 150-180°C. After leaving the laser irradiation region, the fiber temperature decreased gradually for both conditions. No obvious difference was observed between the temperature profiles for 23 MPa and 148 MPa. It should be caused by the cancelation of the heat by plastic deformation and the heat by laser irradiation. To minimize the necking point fluctuation, the lower laser power was chosen for the higher draw ratio and higher drawing stress conditions. Therefore, the increase in the heat of plastic deformation canceled by the decrease of laser irradiation.

3.3. WAXD analysis. Figure 4 shows WAXD images taken at various elapsed times for three drawing stress conditions. The meridional and equatorial intensity profiles are also shown in Figures 5. All the WAXD images for negative elapsed time, representing images of the undrawn fiber, show an amorphous halo. For the three drawing conditions, diffraction images at 0.5 ms, just after necking, showed a meridional streak, corresponding to (001') diffraction of the mesomorphic quasi-smectic fibrillar structure, as discussed in previous reports on PET and PEN fibers.[7-9,11,13] The quasi-smectic fibrillar structure developed within one millisecond after necking, and the fiber structure consisting of a crystalline and amorphous phase sequence was formed by way of this mesophase structure within a few milliseconds after necking.

The amorphous halo was concentrated on the equator just after necking, indicating the orientation of the molecular chain. Almost at the same time, streak-like diffraction appeared on the meridian. The meridian streak nearly disappeared at 6 ms (23 MPa), 3 ms (54 MPa), or 2 ms (148 MPa) after necking, and equatorial diffractions of α(010), β(020), α(100), and β(200)+α(-110) appeared with disappearance of the streak. The overall time was about 10-fold longer than for PET.[7] The crystallites were formed just after the mesophase structure disappeared. This indicates that the quasi-smectic fibrillar structure transformed into a three-dimensional crystal.

For the drawing stress of 23 MPa, the β-crystal was predominant, while only the α-crystal developed for the drawing stress of 148 MPa. It is interesting that the β(020) intensity for the drawing stress of 54 MPa first increased with those of the α-crystal diffractions, showed a maximum at 8-30 ms, and then decreased and almost disappeared in the drawn fiber. In contrast, for the drawing stress of 23 MPa, the β(020) intensity increased monotonically with those of the α-crystal diffractions, and for the drawing stress of 148 MPa, no β(020) diffraction was observed at all. The diffraction angles of the α(010) and β(020) peak do not

change much with elapsed time, while those of α(100) and β(200)+α(-110) obviously shifted to a higher angle. This indicates that both the α- and β-form developed crystallites that shrank mainly in their *a*-axis direction in the cooling process after neck drawing.

3.4. Crystallization Rate. To estimate the crystallization rate, we evaluated the crystallinity index, defined as the ratio of the integral intensity of α(010), α(100), β(200)+α(-110) and β(020) to the total integral intensity for diffraction angles of 3° - 15°. To obtain the integral intensities, equatorial profiles were fitted to four Gaussian function peaks. Figure 6 shows the crystallinity indices obtained from the equatorial X-ray diffraction intensity profile. By assuming one-dimensional heterogeneous nucleation and a crystallization retardation time t_0 after necking, the change in crystallinity x can be described by an Avrami-like equation (5), where K is the crystallization rate, t is the elapsed time after necking, and x_∞ is the crystallinity of the drawn fiber.

$$x = [1 - \exp\{-K(t - t_0)\}]x_\infty \tag{5}$$

The crystallinity index profiles were fitted using equation (5) with the following values; K = 655 s^{-1}, x_∞ = 0.68, and t_0 = 4.0 ms for the drawing stress of 23 MPa, K = 940 s^{-1}, x_∞ = 0.80, and t_0 = 1.0 ms for the drawing stress of 54 MPa, and K = 2210 s^{-1}, x_∞ = 0.83, and t_0 = 0.5 ms for the drawing stress of 148 MPa. While the K and t_0 values for 54 MPa have some uncertainty, nevertheless, the evaluated values can be fitted well by the equation. As the drawing stress increased, t_0 decreased while x_∞ and K increased. This is interesting since K and t_0 did not depend on the draw ratio for the case of PET.[9] For PEN, the difference in K and t_0 may originate from the difference in crystal form developed for different drawing stresses. In particular, orientation-induced crystallization of the β-crystal showing longer neck deformation for 23 MPa may need more induction time and crystallization time compared to

those for the α-crystal.

3.5. Crystal form, size, and d-spacing. The β-crystal fraction was defined as the integral intensity fraction of β(020) in the sum of the equatorial diffractions. The β-crystal fractions are shown in Figure 7. Both α- and β-crystals developed for drawing stresses of 23 and 54 MPa. Both showed a small decreasing trend with elapsed time, in particular in the case of 54 MPa. However, the β-crystal fraction could almost be determined at the beginning of crystallization for the case of 23 MPa. It showed that the mixing ratio of α- and β-crystals was formed at the onset of crystallization, and hardly changed with elapsed time. The resultant β-crystal fraction of 75% was obtained for 23 MPa, which is a fairly high value. The formation of the β-crystal occurred when the crystallization temperature was high, i.e., 200 or 245°C[2,3] and at take-up speeds above 4.5 km/min.[16] However, the low drawing stress (23 MPa) condition generated β-rich crystals without high-temperature annealing or high-speed spinning.

Figure 8 shows *d*-spacings of the α(010), β(020) and α(100) diffractions. Generally, the *d*-spacing decreased gradually after 5 ms, and it was observed that the crystal packing increased with neck drawing and thermal shrinkage effect occurred due to a decrease in fiber temperature. The *d*-spacing of α(100) for the low drawing stress (23 MPa) condition showed a higher shrinkage of 4.5% compared to the other conditions, which indicates that the α-crystal occupying less than about 25% for the low stress of 23 MPa became densely packed along the *a*-axis direction. Figure 9 shows crystallite sizes obtained for the α(010), β(020) and α(100) diffractions. The crystallite sizes of the α-crystal increased gradually with elapsed time for drawing stresses of 54 MPa and 148 MPa. However, for the 23 MPa drawing stress, the crystallite size for the α(010) direction clearly shows a smaller value and a decreasing trend, while the crystallite size of the β-crystal is larger than the other condition and decreases gradually after 10 ms. This indicates the β-crystal formed predominantly just after necking

restrained the development of the α-crystal and after 10 ms, the β-crystallites no longer increased.

3.6. Quasi-smectic fibrillar structure. Sharp (001') diffraction peaks of the mesophase structure were observed before the development of the crystallites. Some studies have reported that the mesophase structure is formed after cold drawing of PEN,[4,6] and some researchers including our group have reported the (001') diffraction of PET by *in situ* analysis during drawing.[8,9,13,15,16] We first communicated the temporal appearance of (001') diffraction, reflecting a quasi-smectic fibrillar structure of PEN.[7] Figure 10 shows the *d*-spacing of meridional (001') diffraction calculated by Bragg's formula for the three drawing stress conditions. The *d*-spacing was almost constant but increased somewhat with elapsed time. This is in contrast to the case of PET,[9] where the *d*-spacing decreased with elapsed time. Longer *d*-spacing was observed for the high drawing stress (148 MPa) condition of PEN. This is also in contrast to the case of PET,[9] which shows no draw rate dependence. Considering the *c*-axis lengths of the α-crystal and the β-crystal of 1.32 nm and 1.273 nm respectively, it is believed that the difference of 3.7% was caused by variation in the (001') *d*-spacing. The maximum *d*-spacings for the drawing stresses of 148 and 23 MPa were 1.27 and 1.23 nm, respectively, where the former is approximately 3.25% longer than the latter. Thus, it is seen that a decrease in applied drawing stress yielded a decrease in the (001') *d*-spacing of the mesophase structure, and when the (001') *d*-spacing is less than a certain value, about 1.25 nm, the β-crystal becomes stable. The mesophase with a longer (001') *d*-spacing resulted in the α-crystal with longer *c*-axis, while a mesophase with shorter (001') *d*-spacing resulted in the β-rich crystal with a shorter *c*-axis. Thus, the (001') diffraction, reflecting the quasi-smectic fibrillar structure of PEN, varied with the drawing stress, and different mesophases led to different mixing ratios of the α- and β-crystal. The (001') *d*-spacing of PET reported previously[9,10,13] is 1.03-1.04 nm, which is shorter than that of PEN, because the chain repeat

length of PEN is larger since it contains a longer naphthalene group than a benzene group in the backbone.

Figure 11 shows the length of the quasi-smectic fibrillar structure along the fiber axis estimated from the half-width of the meridional (001') diffraction using Scherer's formula (Eq. (4)).[9,10] The lengths of the quasi-smectic fibrillar structure are almost uniform for all drawing stress conditions. This corresponded to our previous study[9,10,13] in which the length of the fibrillar structure was almost independent of the draw ratio. This suggests that the size of the mesophase structure is not decided by the drawing conditions, that is, drawing stress, draw ratio, and drawing rate, but is rather decided by the network-structure of the as-spun fiber.

4. Conclusions

The structural development of PEN fibers drawn under three drawing stresses, i.e., 148, 54, and 23 MPa, was analyzed by *in situ* X-ray diffraction and fiber temperature measurements. The drawing stress influenced on the chain conformation of the mesophase structure, and on the resulting crystal form. The longer (001') spacing generated the α-crystal while the comparatively shorter (001') spacing yielded the β-crystal. The (001') spacings of 1.27 and 1.23 nm for the drawing stresses of 148 and 23 MPa, respectively, were somewhat shorter than the *c*-axis lengths of the α- and β-crystals of 1.32 and 1.27 nm, respectively. The structural development behavior obtained in this work is not only valid for laser-heated drawing process used in this study but also valid for conventional high-speed spinning or drawing processes.

Acknowledgments

The synchrotron radiation experiments were performed at the BL40B2 beamline of SPring-8 with the approval of the Japan Synchrotron Radiation Research Institute (JASRI) (Proposal No. 2008A1445). This research was supported by Grant-in-Aid No. 18550191 from the Japan Society for the Promotion of Science.

References

(1) Mencik, Z. *Chem. Prum.* **1967**, *42*, 78.

(2) Buchner, S.; Wiswe, D.; Zachmann, H. G. *Polymer* **1989**, *30*, 480.

(3) Cakmak, M.; Wang, Y. D.; Simhambhatla, M. *Polym. Eng. Sci.* **1990**, *30*, 721.

(4) Jakeways, R.; Klein, J. L.; Ward, I. M. *Polymer* **1996**, *37*, 3761.

(5) Welsh, G. E.; Blundell, D. J.; Windle, A. H. *J. Mat. Sci.* **2000**, *35*, 5225.

(6) García Gutiérrez, M. C.; Karger-Kocsis, J.; Riekel, C. *Macromolecules* **2002**, *35*, 7320.

(7) Kim, K. H.; Aida, R.; Kang, Y. A.; Ohkoshi, Y.; Gotoh, Y.; Nagura, M.; Urakawa, H. *Polymer* **2009**, *50*, 4429.

(8) Yamaguchi, T.; Komoriyama, K.; Ohkoshi, Y.; Urakawa, H.; Gotoh, Y.; Terasawa, N.; Nagura, M.; Kajiwara, K. *J. Polym. Sci. Part B Polym. Phys.* **2005**, *43*, 1090.

(9) Yamaguchi, T.; Kim, K. H.; Murata, T.; Koide, M.; Hitoosa, S.; Urakawa, H.; Ohkoshi, Y.; Gotoh, Y.; Nagura, M.; Kodera, M.; Kajiwara, K. *J. Polym. Sci. Part B Polym. Phys.* **2008**, *46*, 2126.

(10) Kim, K. H.; Kang, Y. A.; Murata, T.; Ikehata, S.; Ohkoshi, Y.; Gotoh, Y.; Nagura, M.; Koide, M.; Urakawa, H.; Kotera, M. Polymer **2008**, *49*, 5705.

(11) Kim, K. H.; Yamaguchi, T.; Ohkoshi, Y.; Gotoh, Y.; Nagura, M.; Urakawa, H.; Kodera, M.; Kikutani, T. *J. Polym. Sci. Part B Polym. Phys.* **2009**, *47(17)*, 1653.

(12) Kang, Y. A.; Kim, K. H.; Ikehata, S.; Ohkoshi, Y.; Gotoh, Y.; Nagura, M.; Koide, M.;

Urakawa, H. *Polym. J.* **2010**, *42*, 657.

(13) Kim, K. H.; Murata, T.; Kang, Y. A.; Ohkoshi, Y.; Gotoh, Y.; Nagura, M.; Urakawa, H. *Macromolecules* **2011**, *44*, 7378.

(14) Aida, R.; Kim, K. H.; Ikehata, S.; Kang, Y. A.; Ohkoshi, Y.; Gotoh, M.; Nagura, M. *Fiber preprint* **2008**(June 18-20), 58.

(15) Hsiao, B. S.; Kennedy, A. D.; Leach, R. A.; Cho, B.; Harney, P. *J. Appl. Crystallogr.* **1997**, *30*, 1084.

(16) Ran, S.; Wang, Z.; Burger, C.; Chu, B.; Hsiao, B. S. *Macromolecules* **2002**, *35*, 10102.

Figure Captions

Fig. 1 Schematic diagrams of in situ WAXD measurement system (a) and three-directional irradiation by mirror unit (b).

Fig. 2 Photographs captured around the necking location for drawing stress of (a) 23 MPa, (b) 54 MPa, and (c) 148 MPa.

Fig. 3 Fiber temperature profiles.

Fig. 4 WAXD images taken for the noted elapsed time on the neck-drawing of PEN fiber. Drawing stresses is also noted.

Fig. 5 Intensity profiles taken for the noted elapsed time during the neck-drawing of PEN fiber under the drawing stress of (a) 23 MPa, (b) 54 MPa, and (c) 148 MPa.

Fig. 6 Crystallinity indices estimated for the equatorial intensity profiles. Fitting curves of Eq.(5) were also shown.

Fig. 7 β-crystal fraction estimated by the integral intensity fraction of β(020) in the sum of equatorial diffractions.

Fig. 8 d-spacing of α(010) (a), β(020) (b), and α(100) (c).

Fig. 9 Crystallite sizes of α(010) (a), β(020) (b), and α(100) (c).

Fig. 10 d-spacing of (001') diffraction plotted against the elapsed time after necking.

Fig. 11 Persistence length estimated by the peak width of (001') diffractions.

Table 1 Drawing conditions

Condition	Drawing stress (MPa)	Draw ratio	Take-up speed (m/min)	Laser power (W)
1	148	7.5	22.5	2.5
2	54	7.0	28.0	2.6
3	23	5.5	30.0	3.3

Graphical Abstract

Drawing Stress /MPa	d(001') /nm	β-fraction /%
148	1.27	0
54	1.26	11
23	1.23	74

Figures

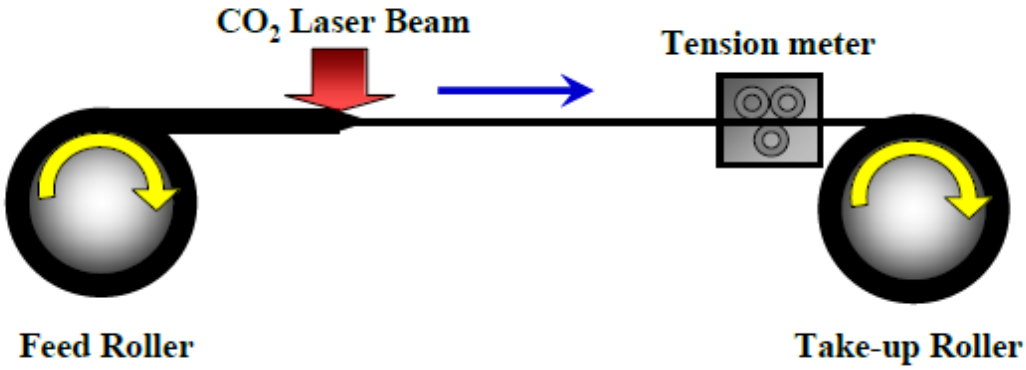

(a)

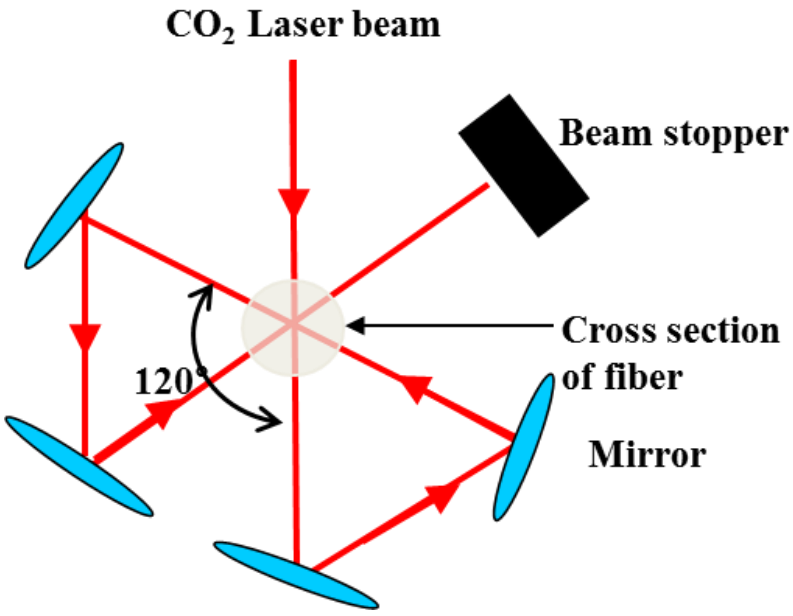

(b)

Fig. 1 Schematic diagrams of *in situ* WAXD measurement system (a) and three-directional irradiation by mirror unit (b).

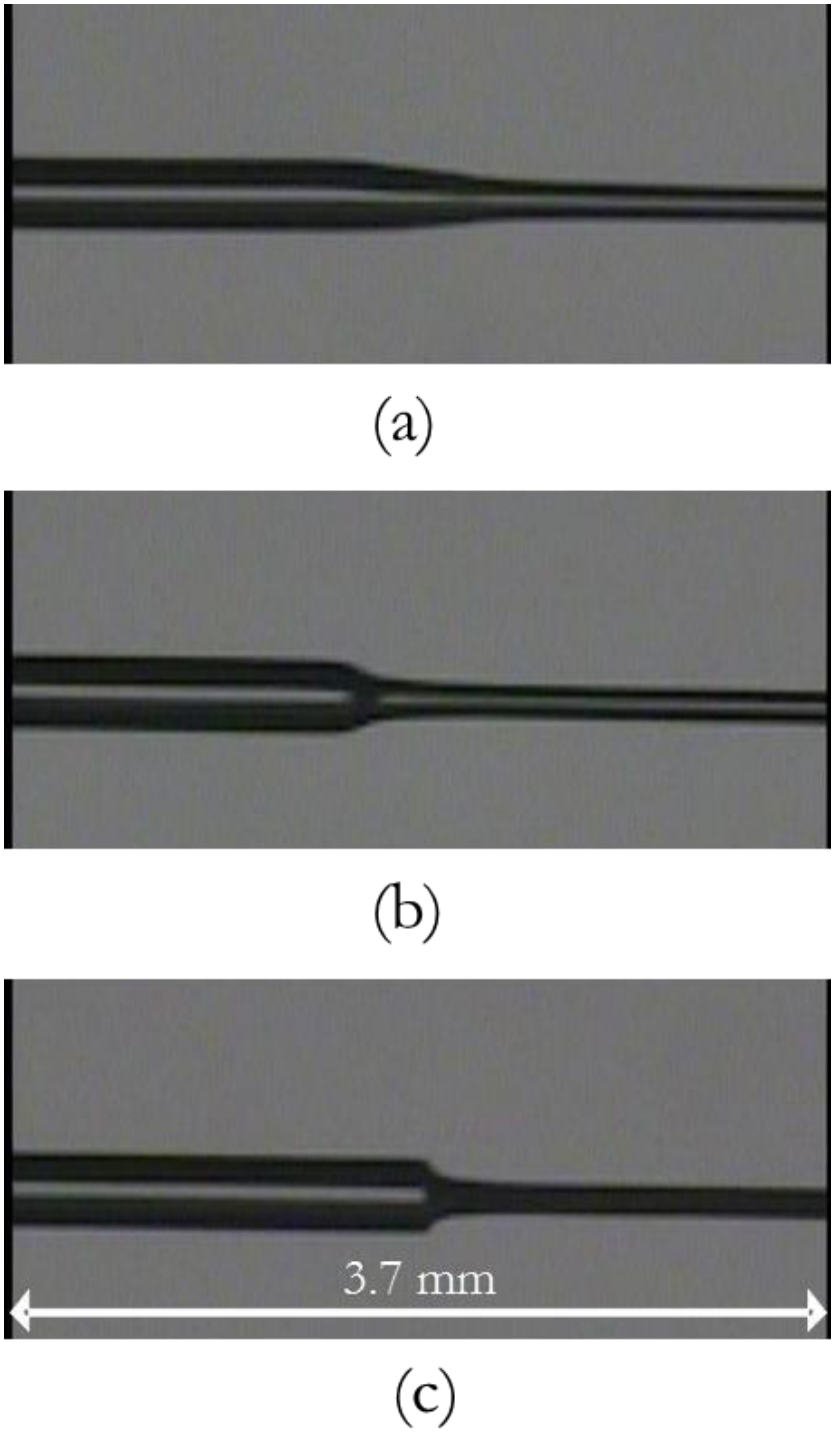

Fig. 2 Photographs captured around the necking location for drawing stress of (a) 23 MPa, (b) 54 MPa, and (c) 148 MPa.

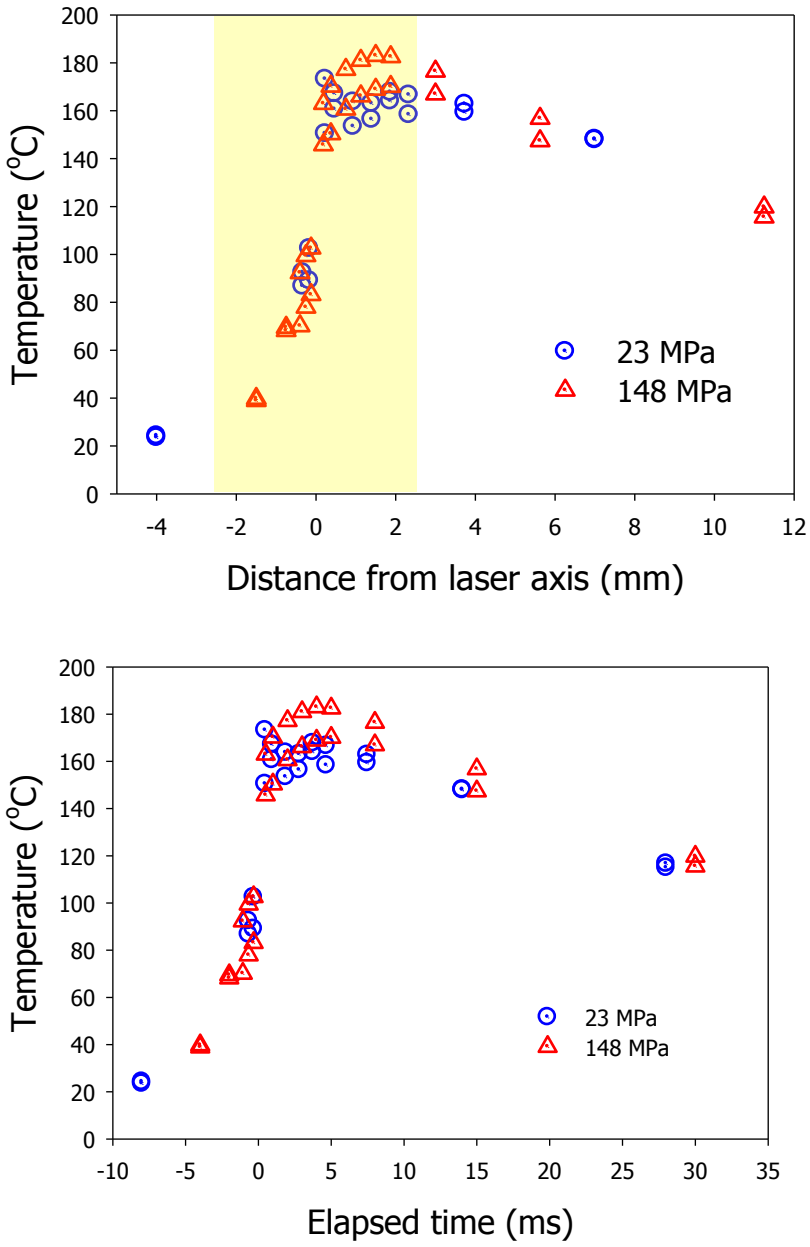

Fig. 3 Fiber temperature profiles.

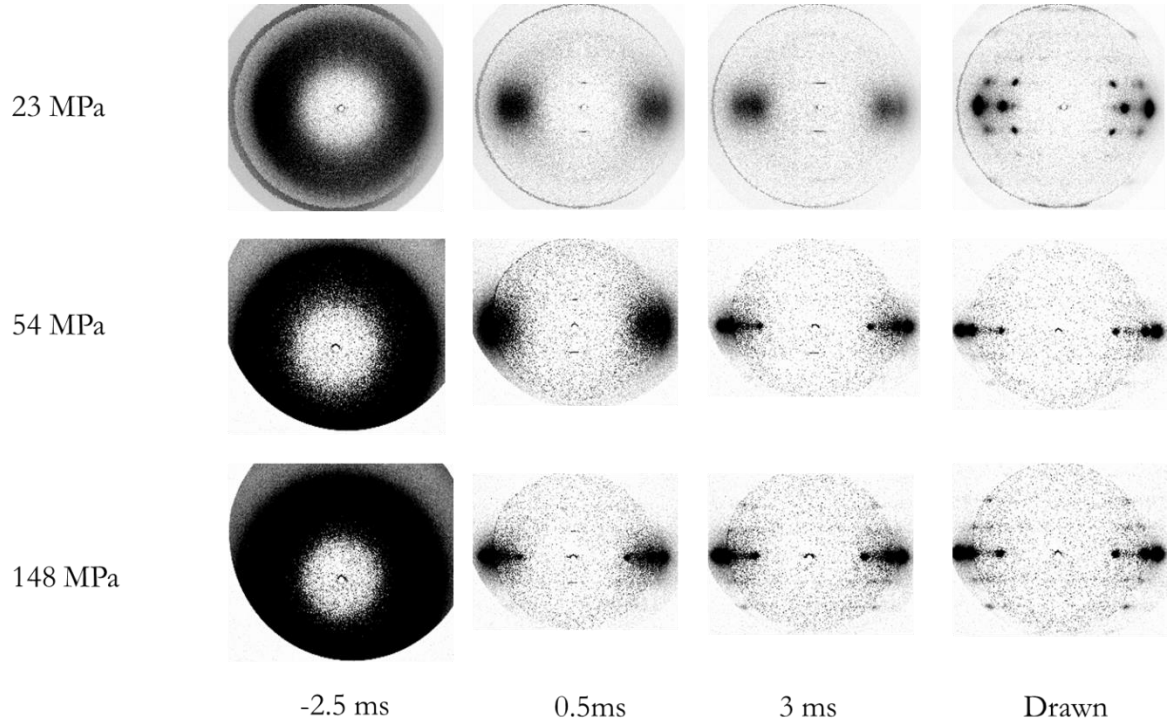

Fig. 4 WAXD images taken for the noted elapsed time on the neck-drawing of PEN fiber. Drawing stresses is also noted.

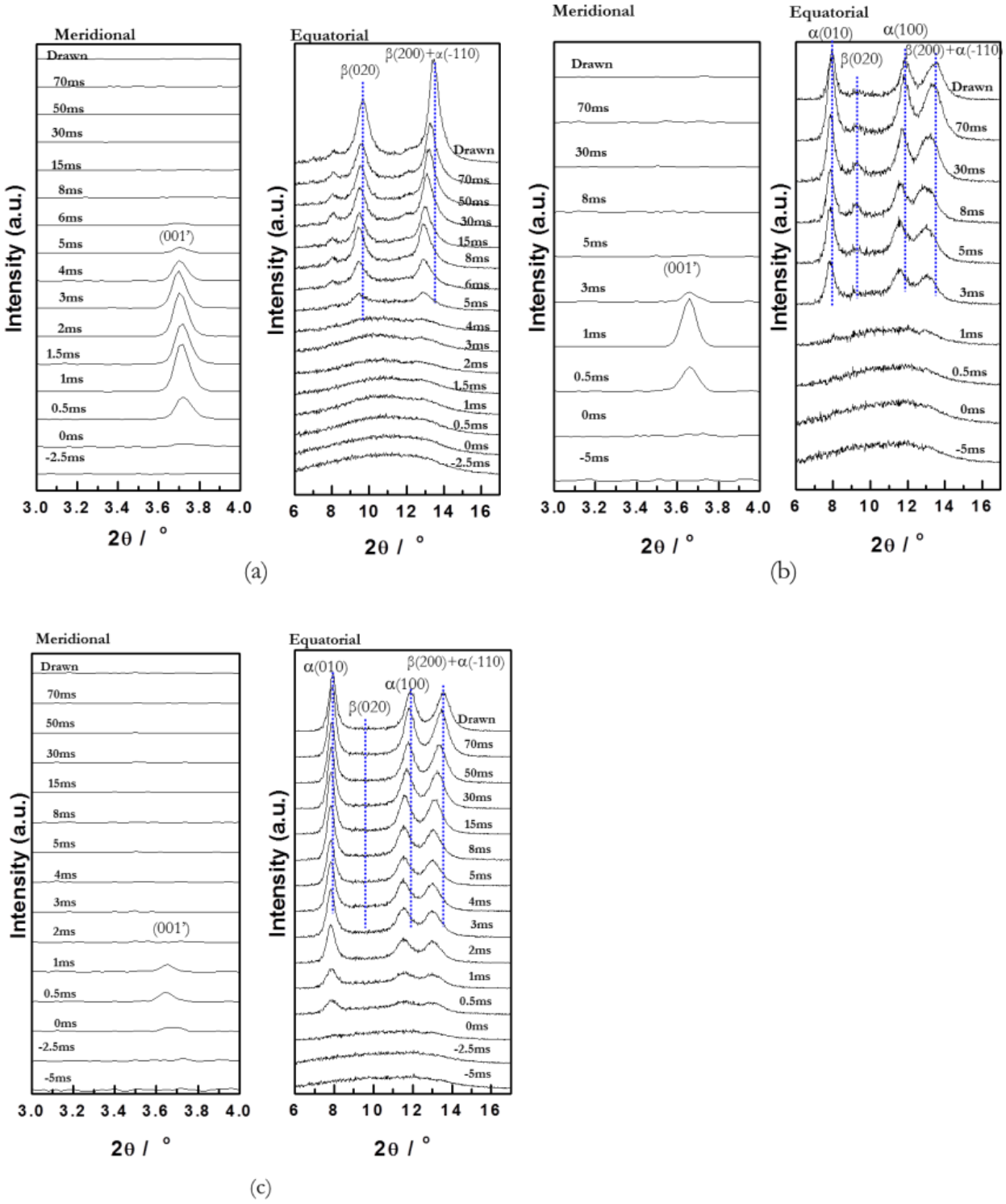

Fig. 5 Intensity profiles taken for the noted elapsed time during the neck-drawing of PEN fiber under the drawing stress of (a) 23 MPa, (b) 54 MPa, and (c) 148 MPa.

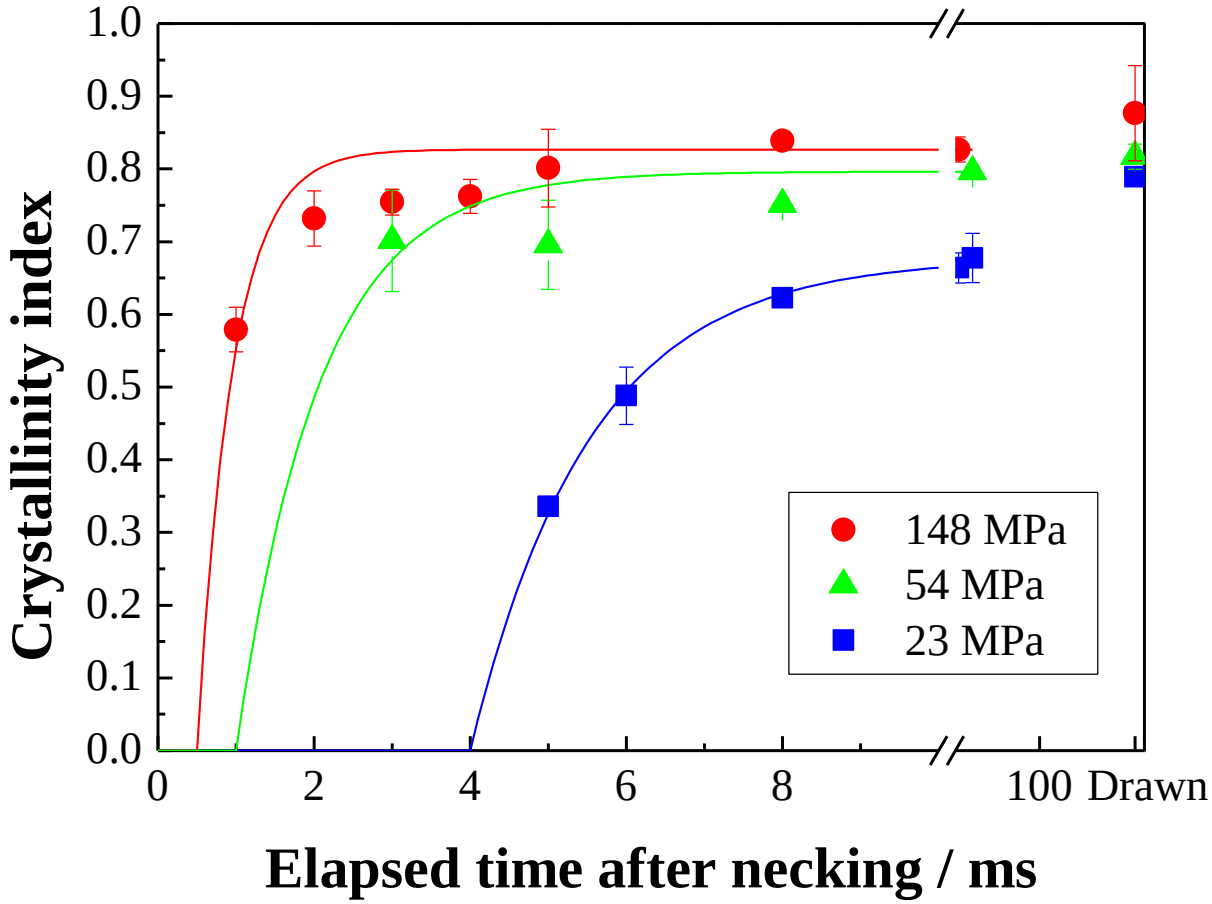

Fig. 6 Crystallinity indices estimated for the equatorial intensity profiles. Fitting curves of Eq.(5) were also shown.

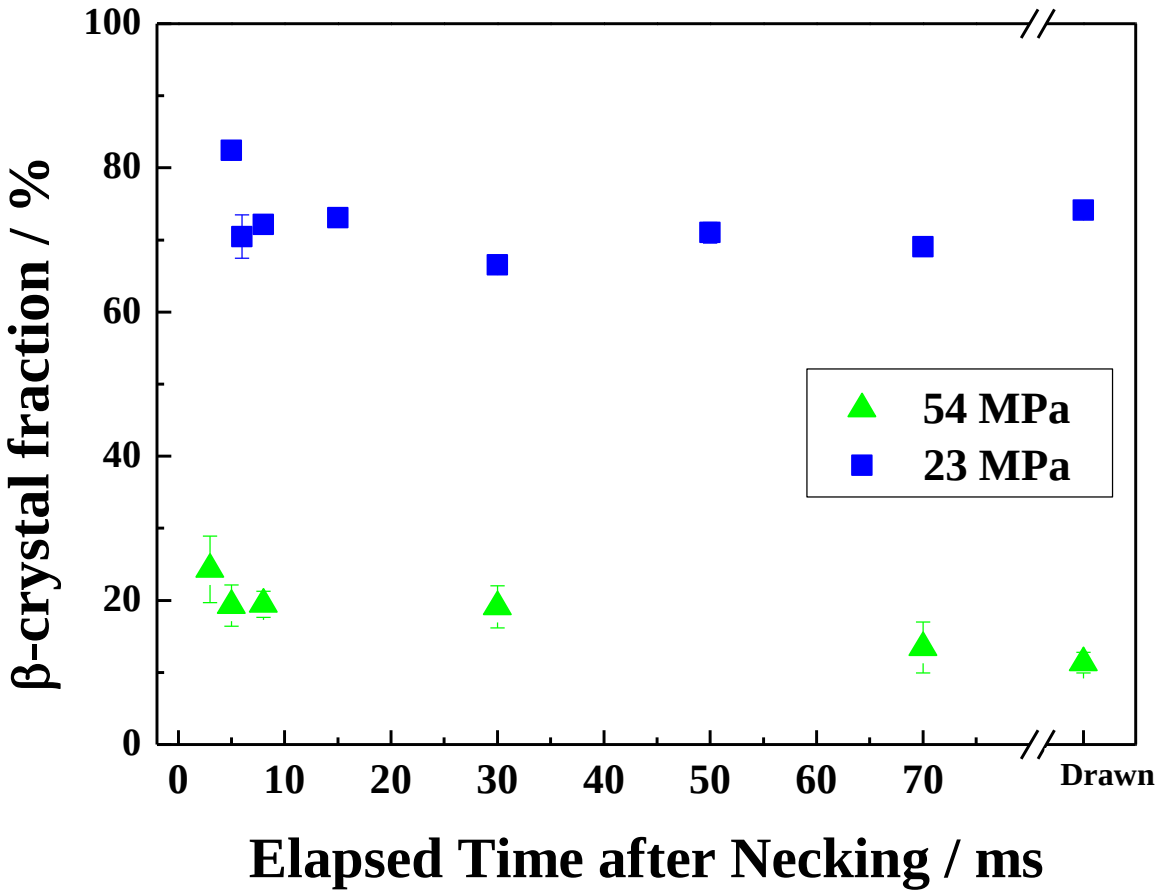

Fig. 7 β-crystal fraction estimated by the integral intensity fraction of β(020) in the sum of equatorial diffractions.

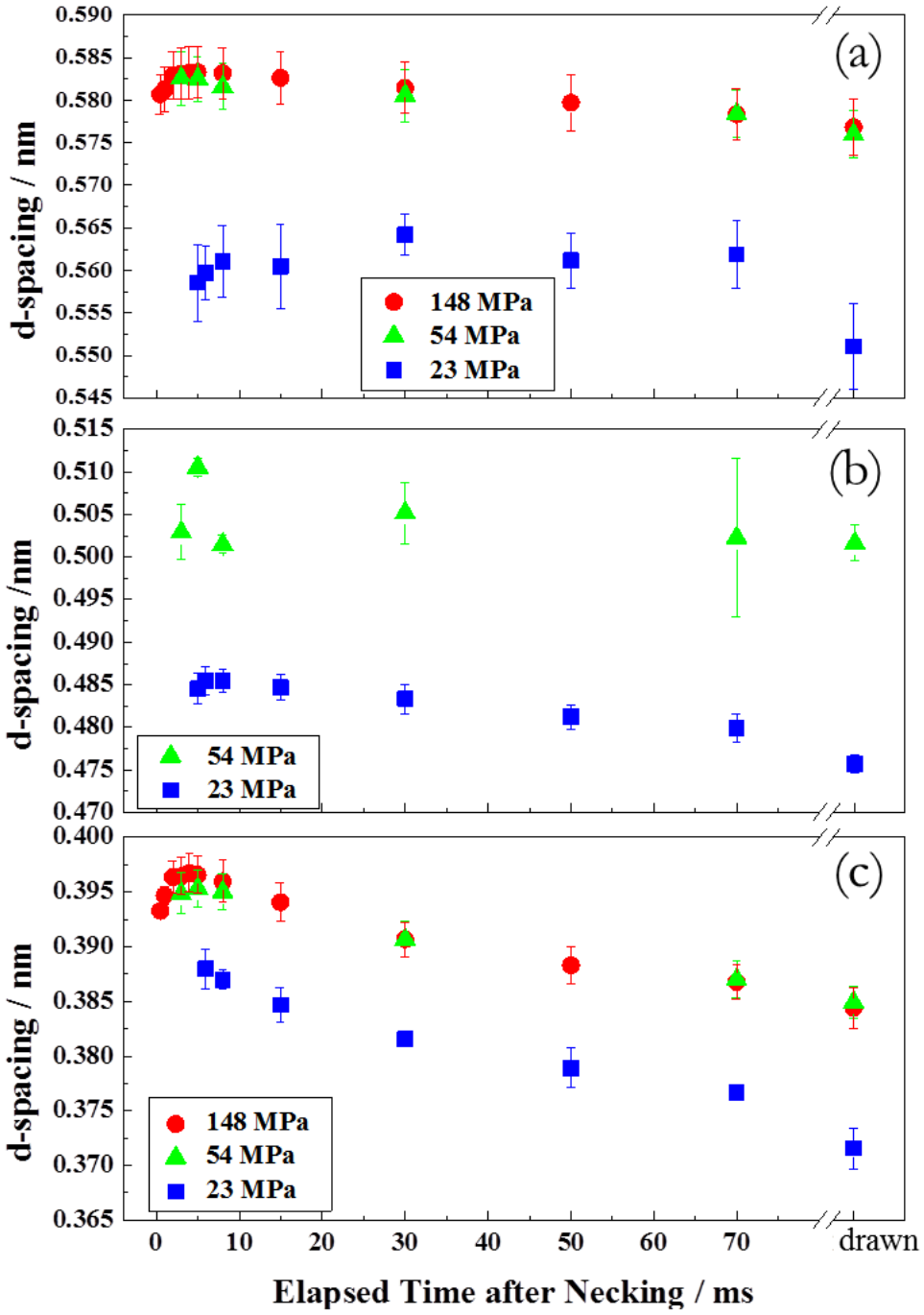

Fig. 8 *d*-spacing of α(010) (a), β(020) (b), and α(100) (c).

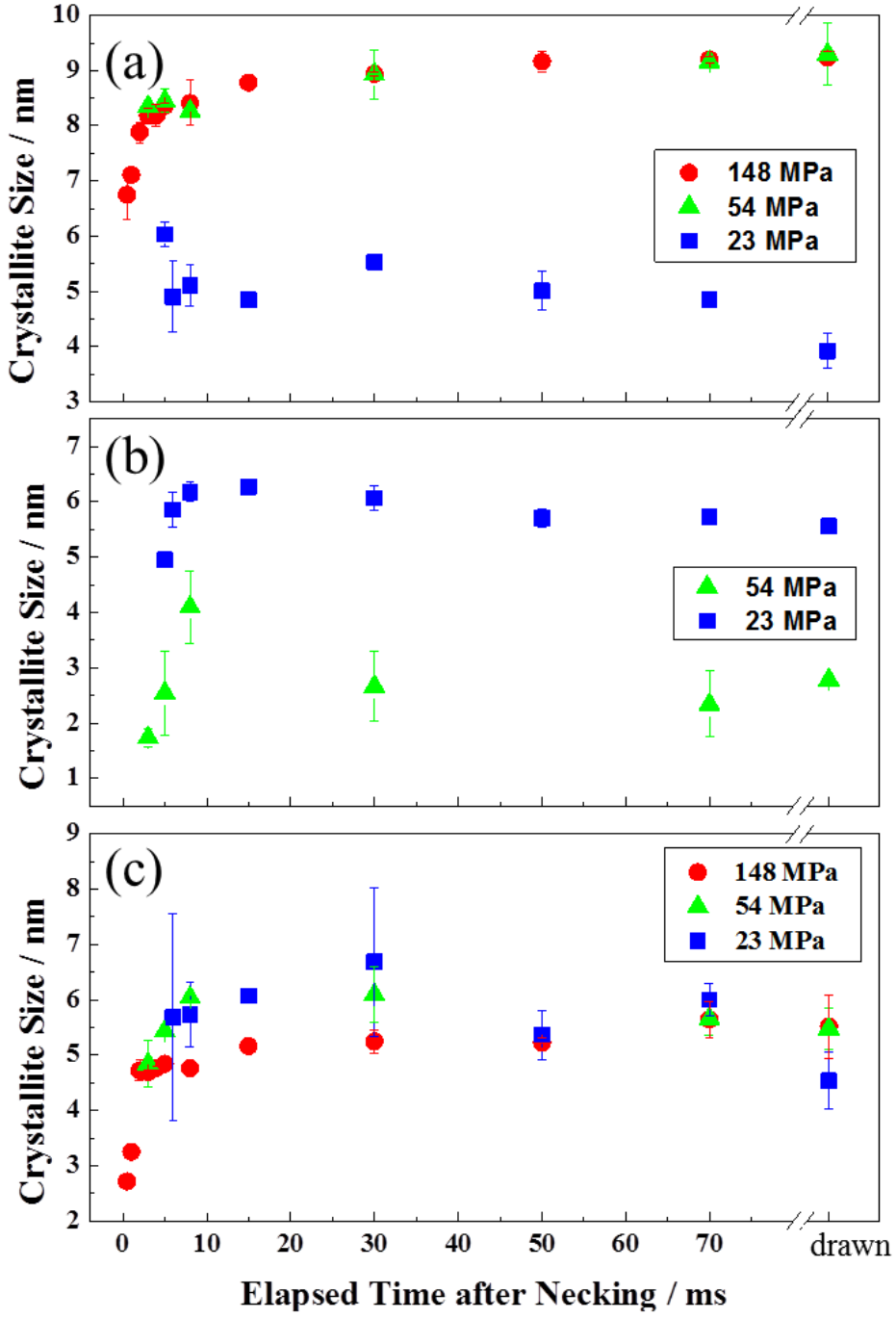

Fig. 9 Crystallite sizes of α(010) (a), β(020) (b), and α(100) (c).

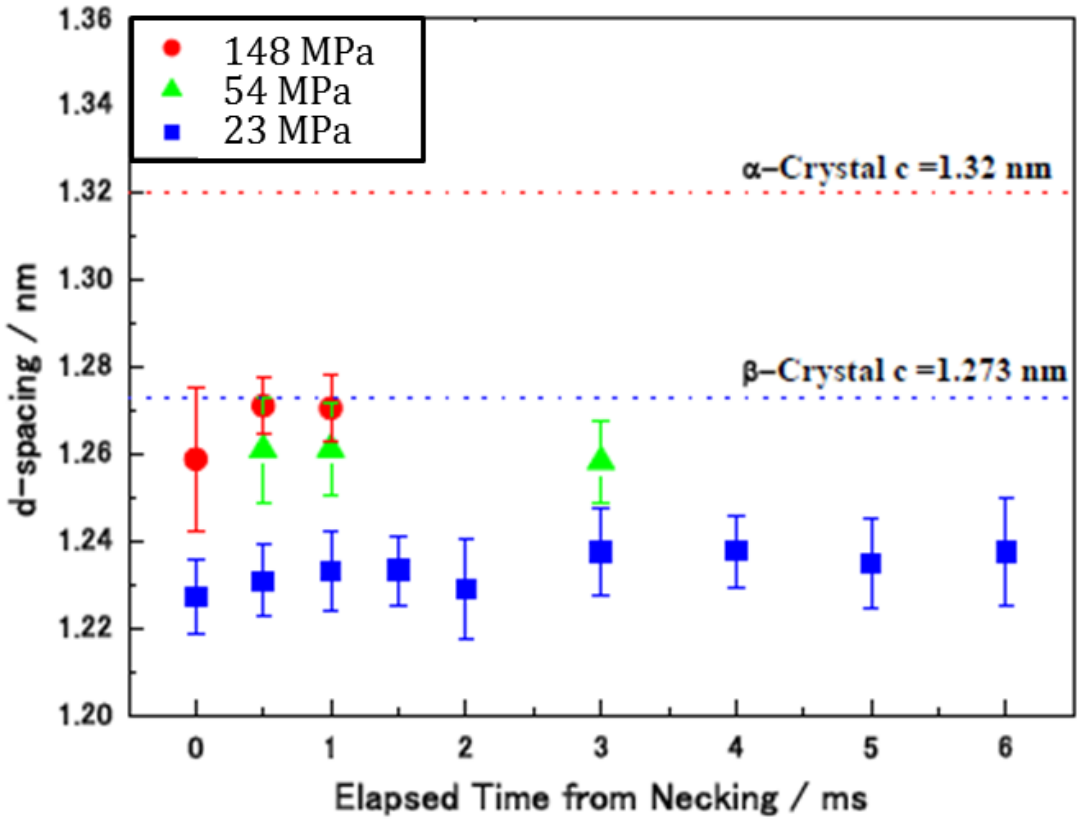

Fig. 10 d-spacing of (001') diffraction plotted against the elapsed time after necking.

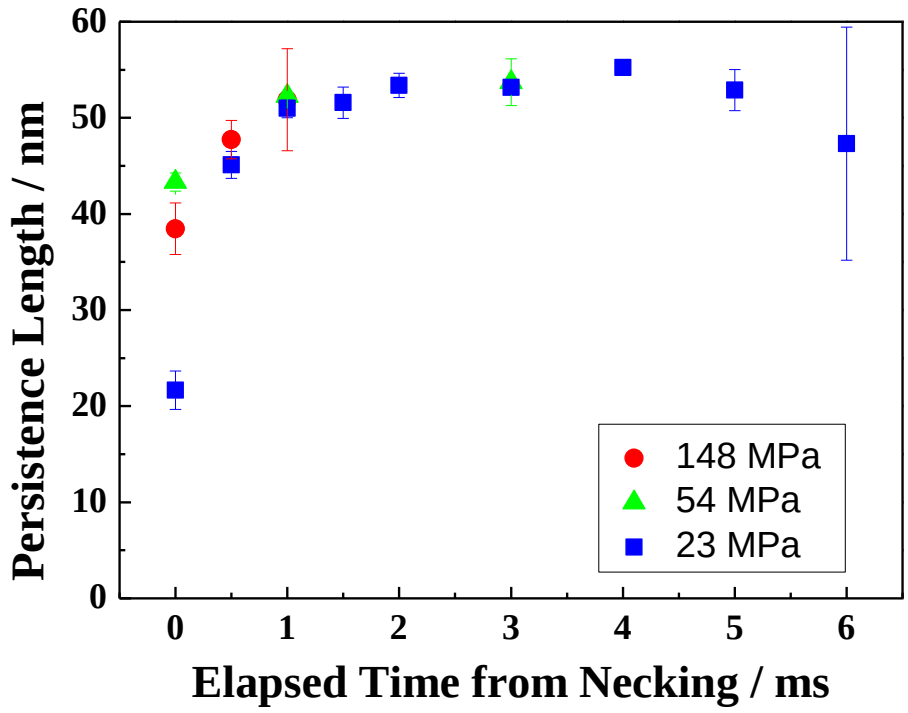

Fig. 11 Persistence length estimated by the peak width of (001') diffractions.